

Hybrid Energy Storage Module in Photovoltaic Power Generation System for Brushless DC Motor Operation

Hung-Cheng Chen,¹ Shin-Shiuan Li,¹ and Shing-Lih Wu^{2*}

¹Prospective Technology of Electrical Engineering and Computer Science,
National Chin-Yi University of Technology, No. 57, Sec. 2, Zhongshan Rd., Taiping Dist., Taichung 411030, Taiwan

²Department of Electrical Engineering, National Taitung Junior College,
No. 889, Jhengci N. Rd., Taitung 95045, Taiwan

(Received September 6, 2021; accepted January 11, 2022)

Keywords: photovoltaic power generation, hybrid energy storage module, uninterruptible power supply, supercapacitor, lithium-ion battery

Photovoltaic power generation systems often suffer from voltage instability and intermittent production of electricity due to shade, dust, rain, and so forth, resulting in unstable power quality. Such problems of photovoltaic power generation systems cause the malfunction of devices connected to the system, especially in systems with brushless DC motors. To solve these problems, a hybrid energy storage module and a precise control strategy for photovoltaic power generation systems are proposed. The system comprises solar cells, a hybrid energy storage module, a power conversion module, a sensing-type pyrheliometer, and a brushless DC motor. The hybrid energy storage module is composed of a supercapacitor and a lithium-ion battery, which are connected in parallel. The power conversion module includes a maximum power point tracking converter, a boost converter, a controller, and switches. The sensing-type pyrheliometer monitors the luminous intensity during operation, which enables the controller to analyze the signals of the system and control the system through the terminal voltage of the hybrid energy storage module. A brushless DC motor is connected to the system to investigate by how much the power quality and operation time are improved. The experimental results show that the system has a sustainable power supply because the brushless DC motor operates for up to 342 s without any interruption, longer than that for a photovoltaic system with a supercapacitor only. Thus, the photovoltaic power generation system with the proposed hybrid energy storage module and the control strategy effectively reduces the voltage instability and the interruption of power generation and improves the quality of the power.

1. Introduction

Renewable energy from the Sun is available through photovoltaic power generation and helps to reduce the use of fossil fuels and environmental pollution.^(1–5) A supercapacitor is mainly used for photovoltaic power generation as it plays an important role as a secondary power supply and in power storage by providing a strong pulse power.^(6–9) A supercapacitor is an

*Corresponding author: e-mail: lihchoug@ntc.edu.tw
<https://doi.org/10.18494/SAM3648>

electrochemical element in which a reversible chemical reaction occurs and is presently regarded as a new energy storage device.^(10–12) In a supercapacitor, power charging and storage are carried out by the active electrode, the electrolyte, and the interface through the double-layer structure. Several potential applications of supercapacitors for uninterrupted power supply systems, fast start applications, peak pulse power supply applications, fast charging applications, memory backup applications, and so forth have been reported.^(13–18) Lithium-ion batteries are also widely used for photovoltaic power generation because of their sufficient power storage capacity, low self-discharge rate, high working voltage, and high energy density.^(19,20)

A brushless DC motor is used with a photovoltaic power generation system owing to its fast start, small size, high reliability, and long life.^(21–25) However, to operate a brushless DC motor with a photovoltaic power generation system effectively, the problems of irregular power output and voltage instability due to shade, dust, and other weather conditions must be solved.

Therefore, we propose a hybrid energy storage module with a supercapacitor and lithium-ion batteries as an energy storage device for a photovoltaic power generation system to supply power to a brushless DC motor. Because the proposed hybrid energy storage module contains a supercapacitor and a lithium-ion battery in parallel, the high energy density of the lithium-ion battery compensates for the slow-wave power generation of the supercapacitor, while the supercapacitor eliminates fluctuations and reduces the stress of the battery caused by frequent transient power fluctuations that shorten the life of the lithium-ion batteries. We also propose an appropriate control strategy for the hybrid energy storage module.

Our experimental results show that the hybrid energy storage module with the proposed control strategy provides an uninterruptible and stable power supply. The proposed hybrid energy storage module prolongs the operation time of the brushless DC motor to 342 s. The photovoltaic power generation system with the proposed module reduces the intermittency of power production and the instability of the system, allowing the stable and prolonged operation of a brushless DC motor connected to the photovoltaic power generation system.

2. System Specification

A brushless DC motor is connected to a photovoltaic power generation system that consists of a photovoltaic module, a hybrid energy storage module, a power conversion module, and a sensing-type pyrheliometer. The system has a hybrid energy storage module composed of a supercapacitor and a lithium-ion battery connected in parallel (Fig. 1). The power conversion module consists of a maximum power point tracking (MPPT) converter, a boost converter, a controller, and switches.

2.1 Photovoltaic module

A TYNP62610260 photovoltaic module (Tynsolar Corporation, Taiwan) is used. Its maximum power is 260 W. In the experimental process, two photovoltaic modules are included in the system.

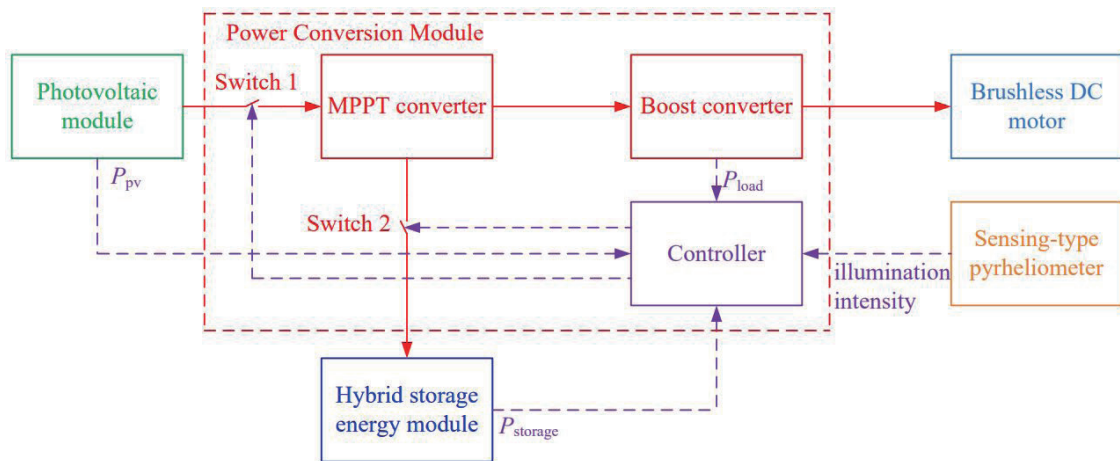


Fig. 1. (Color online) System structure of the solar-based hybrid energy storage module with brushless DC motor operation.

2.2 Maximum power point tracking converter

The input voltage of the MPPT converter in the system is in the range of 7–40 V, the output voltage is in the range of 7–29 V, and the maximum charging current is 26 A. For the experiment, the output of the MPPT converter is set to a fixed value of 24 V for the lithium-ion battery module in the hybrid energy storage module. The photovoltaic module with the MPPT converter supplies the generated power to the hybrid energy storage module.

2.3 Boost converter

The input voltage of the boost converter in the system is from 12 to 60 V and the output is a fixed voltage of 48 V. The converter provides a maximum power of 2 kW. When the hybrid energy storage module discharges power, the boost converter increases its working voltage to 48 V and supplies it to the brushless DC motor to prolong its operation time.

2.4 Supercapacitor

A BMOD0165 P48V C01 supercapacitor (Maxwell Technologies, Inc., Hong Kong) is used. It has an output voltage of 48 V and a capacitance of 165 F.

2.5 Lithium-ion batteries

Eight 40138-type lithium-ion batteries are used in the system, each of which has a voltage of 3.3 V and a capacity of 10 Ah. The batteries charge the energy storage module with a maximum voltage and current of 26.4 V and 10 Ah, respectively.

2.6 Programmable logic controller (PLC)

An MSP430 controller receives signals from the sensing-type pyrheliometer, photovoltaic module, boost converter, and hybrid energy storage module. The power of the photovoltaic power generation system is analyzed by using the data received from the sensing-type pyrheliometer. The controller decides the electricity production, the load power of the photovoltaic module, and the switching on or off.

2.7 Sensing-type pyrheliometer

To determine the current luminous intensity, the relationship between the output of the solar cell and luminous intensity needs to be known as shown in Fig. 2. The output current of the solar cell is proportional to the luminous intensity of the Sun; the stronger the sunlight, the higher the output power of the solar cell. Upon a decrease in luminous intensity, the shape of the I - V curve remains unchanged but the short-circuit current decreases gradually. The open-circuit voltage changes little with the luminous intensity. The sensing-type pyrheliometer is designed to contain a small solar cell and a transconductance amplifier. Owing to the characteristics of the amplifier, the open-loop voltage gain of an ideal operational amplifier is infinite. When an operational amplifier circuit performs linear amplification, $V_i = -V + V = 0$. Therefore, the two input ends form a short circuit, that is, $-V = +V$ as the input impedance Z_i is infinite and there is no current at both ends. If one end is grounded, the circuit is virtually grounded. Figure 3 shows the circuit of the sensing-type pyrheliometer used in the proposed module, which measures the short-circuit current of the solar cell and converts the current into a voltage signal for the PLC to measure the luminous intensity. The active directory module of the PLC ranges from 0 to 10 V, and the feedback resistance R_f is adjusted to make the maximum irradiance of the amplifier output at the given position equal to 10 V.

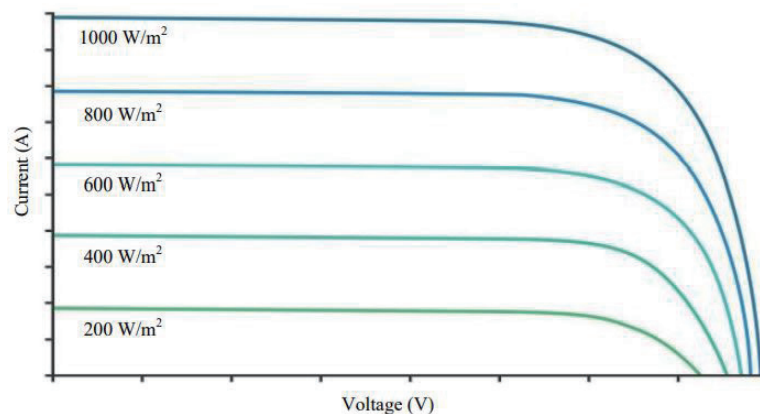


Fig. 2. (Color online) I - V curve of the solar cell.

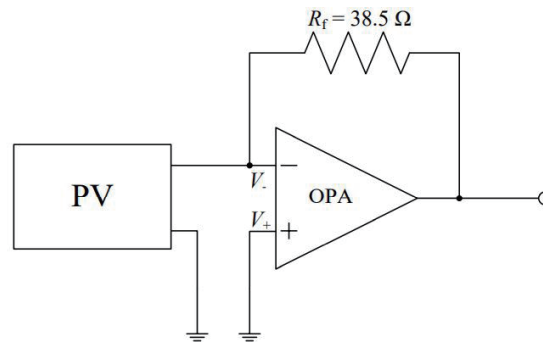


Fig. 3. Circuit of sensing-type pyrheliometer.

2.8 Brushless DC motor and electromagnetic clutch

A brushless DC motor with a rated voltage of 48 V and rated power of 780 W is connected to the photovoltaic power generation system. To simulate the power load and control the loading condition, an electromagnetic clutch (ZKC1S2AA) is added to the brushless DC motor.

3. Control Strategies of Hybrid Energy Storage Module

The operation principle of the hybrid energy storage module is briefly described as follows. The controller receives the signals of luminous intensity and the powers of the photovoltaic module (P_{pv}), boost converter (P_{load}), and hybrid energy storage module ($P_{storage}$). It implements an appropriate control strategy, as shown in Fig. 4. On the basis of the received data, the controller operates the system and reduces the voltage instability and intermittency of the output photovoltaic generated power. This helps to secure power supply continuity and improve the quality of the output power. The different control strategies and switch arrangements are shown in Table 1.

3.1 Control strategy 1

If luminous intensity $\geq 530 \text{ W/m}^2$, the system starts. Then, when $P_{pv} > P_{load}$, switch 1 is turned on to transfer sufficient energy to the MPPT converter, and from the converter to the brushless DC motor. If there is excess power, switch 2 is turned on so that the remaining energy $P_{pv} - P_{load}$ is supplied to the hybrid energy storage module for charging.

3.2 Control strategy 2

When $P_{pv} < P_{load}$, switch 1 is turned off. At this time, the photovoltaic module does not generate power. If the controller judges that $P_{storage} - P_{load}$ is sufficiently large to operate the brushless DC motor, then switch 2 is turned on, and the hybrid energy storage module supplies power to the system.

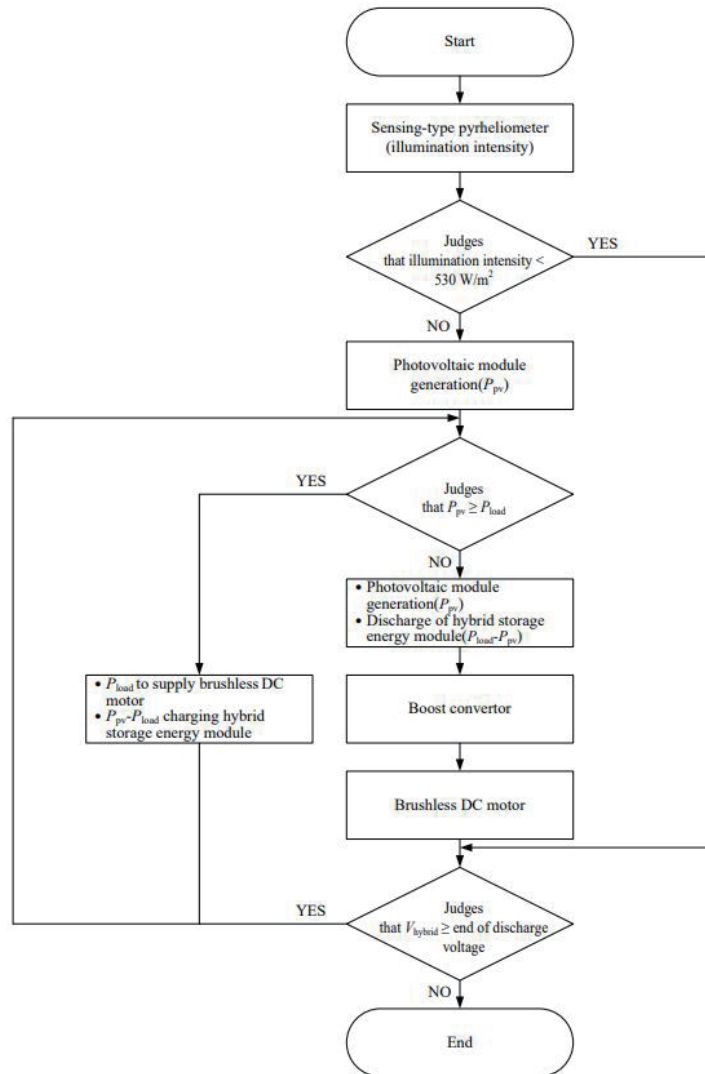


Fig. 4. Operation flow chart of the solar-based hybrid energy storage module.

Table 1
Control strategies.

Control strategy	Luminous intensity (W/m ²)	Judgment mode	Switch 1	Switch 2
1	≥530	$P_{pv} > P_{load}$	ON	ON
2	≥530	$P_{pv} < P_{load}$ but $P_{storage} > P_{load}$	OFF	ON
3	≥530	$P_{pv} = P_{load}$	ON	OFF
4	<530	$P_{pv}, P_{storage} < P_{load}$	OFF	OFF

3.3 Control strategy 3

When $P_{pv} = P_{load}$, switch 1 is turned on to transfer sufficient energy to the MPPT converter and then to the brushless DC motor. However, in this case, the power is only sufficient to be supplied to the brushless DC motor, so switch 2 is turned off.

3.4 Control strategy 4

If luminous intensity $< 530 \text{ W/m}^2$, the system does not start. However, to avoid misjudgment, the system operation is decided at the second stage. When $P_{pv} < P_{load}$, switches 1 and 2 are turned off. Then, the solar hybrid energy storage module has no energy supply, so the system is shut down. At this time, P_{load} and $P_{storage}$ are sent to the controller to operate the switches.

4. Results and Discussion

4.1 Hybrid energy storage module

In the experiment, only control strategies 1 and 2 are implemented. In control strategy 3, the energy of the photovoltaic module is only sufficient to be supplied to the brushless DC motor. In control strategy 4, the power from the photovoltaic module and hybrid energy storage module is insufficient to operate the brushless DC motor, so the system is completely shut down. Therefore, control strategies 3 and 4 are not considered. The overall operation of the hybrid energy storage module with control strategies 1 and 2 is investigated, and the results are shown in Fig. 5. For control strategy 1, the voltage and current recorded as functions of time are shown in Fig. 6. The result is discussed for five time intervals as follows.

(1) $t < t_0$

The voltage is 33.2 V when the photovoltaic module is added. At this stage, the system has just started, so the voltage does not reach the set value. The change in the voltage with time is shown in Fig. 7.

(2) $t_0 \leq t < t_1$

When $t = t_0$, the brushless DC motor maintains a stable voltage of 47.5 V. This means that the output of the MPPT converter is only connected to the motor. At this time, the voltage of the photovoltaic module is still 33.2 V and the hybrid energy storage module does not operate. When $t_0 < t < t_1$, the motor maintains a stable voltage. As the output of the MPPT converter is not

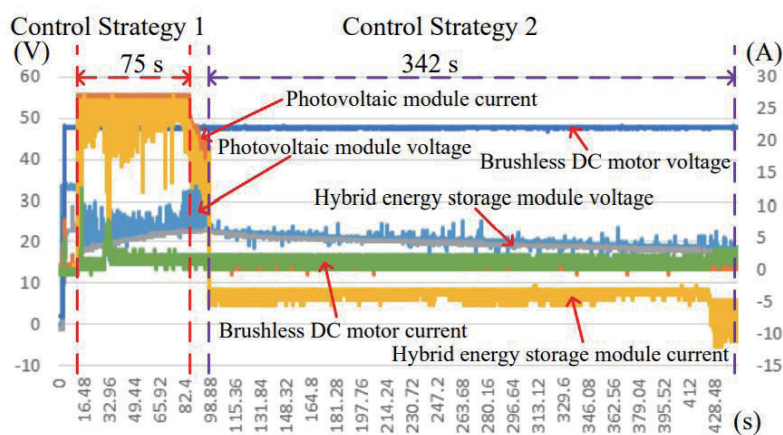


Fig. 5. (Color online) Measurement waveforms of the solar-based hybrid energy storage module.

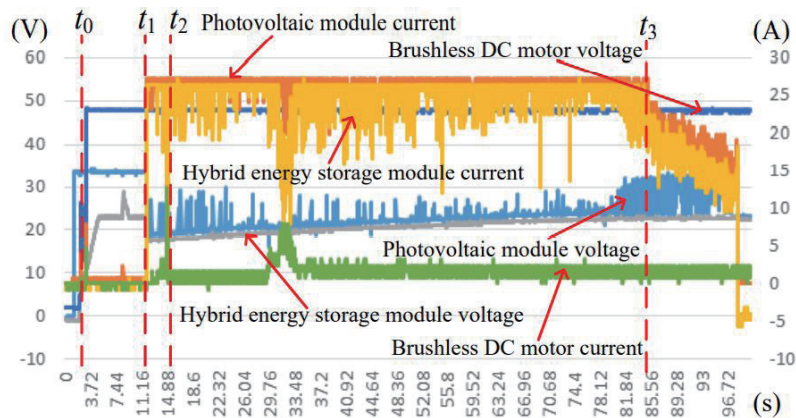


Fig. 6. (Color online) Control strategy 1 of the solar-based hybrid energy storage module.

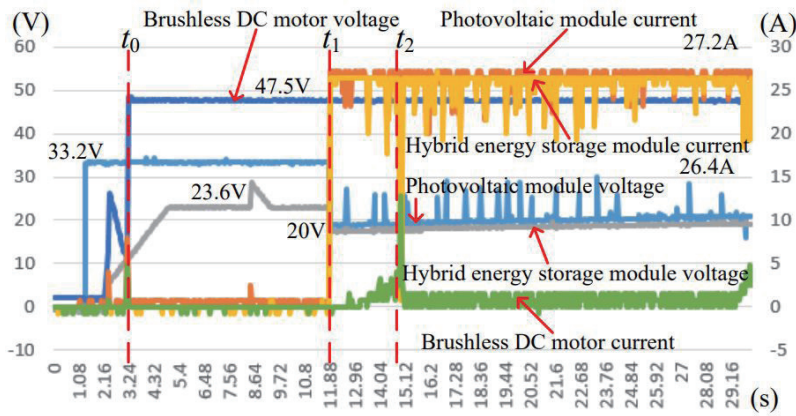


Fig. 7. (Color online) Control strategy 1: $t_0 \leq t < t_2$.

connected to the hybrid energy storage module, the output voltage of the MPPT converter becomes 23.6 V (Fig. 7).

(3) $t_1 \leq t < t_2$

When $t = t_1$, the hybrid energy storage module is connected to the MPPT converter. The initial charging voltage is about 20 V and the current is 27.2 A. The current of the hybrid energy storage module is 26.4 A. When the voltage of the photovoltaic module is affected by the hybrid energy storage module, it drops to 20 V. At this time, the hybrid energy storage module has the maximum charging current. Then, when $t_1 < t < t_2$, the brushless DC motor starts to increase the working current gradually and maintains a voltage of 47.5 V. In this interval, the hybrid energy storage module is charged as shown in Fig. 7.

(4) $t_2 \leq t < t_3$

When $t = t_2$, the operating current increases to the maximum load of the brushless DC motor. The brushless DC motor voltage remains at 47.5 V. Then, when $t_2 < t < t_3$, the electromagnetic clutch is applied to the brushless DC motor. Then, the current of the brushless DC motor reaches 8 A and the voltage is maintained at 47.5 V (Fig. 8). When $t_2 \leq t < t_3$, the hybrid energy storage

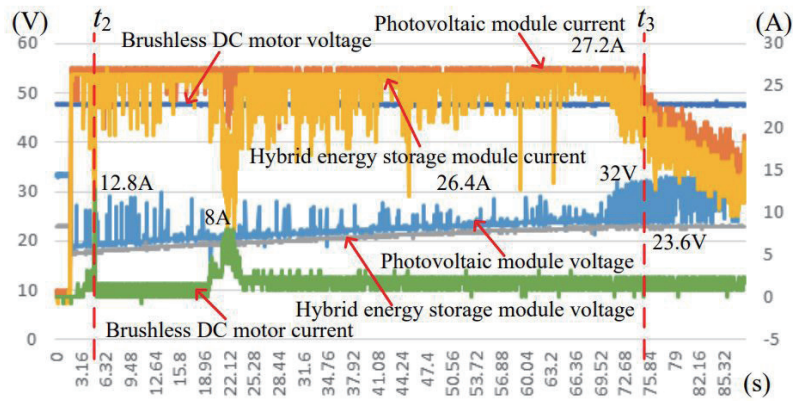


Fig. 8. (Color online) Control strategy 1: $t_2 \leq t < t_3$.

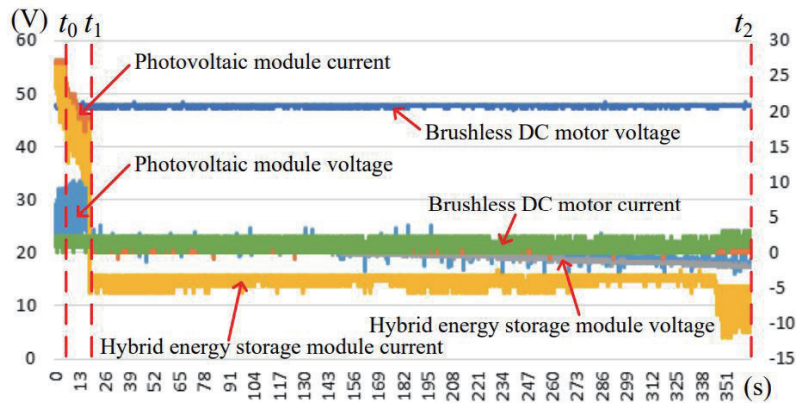


Fig. 9. (Color online) Control strategy 2 of the solar-based hybrid energy storage module.

module is charged while the brushless DC motor is operated at the required voltage. Then, P_{pv} of the system becomes greater than P_{load} .

(5) $t \geq t_3$

When $t \geq t_3$, the current of the energy storage module gradually decreases while the hybrid energy storage module is fully charged to a voltage of 23.6 V. At this time, the brushless DC motor is still operating at the voltage of the photoelectric module of 32 V and the current of 27.2 A. The current does not remain at the same value due to the characteristics of the brushless DC motor (Fig. 8). When $P_{pv} > P_{load}$, the system charges the hybrid energy storage module and maintains sufficient power to operate the motor. When the initial voltage of the hybrid energy storage module reaches 23.6 V, the charging time is about 75 s.

For control strategy 2, the voltage and current are recorded as functions of time as shown in Fig. 9 in three intervals.

(1) $t < t_0$

When $t < t_0$, the current of the hybrid energy storage module decreases gradually while it is charged fully to a voltage of 23.6 V. The voltage of the photovoltaic module is 32 V and the

current is 27.2 A when the brushless DC motor operates. The voltage of the brushless DC motor is 47.5 V and its current hardly changes with time (Fig. 10).

(2) $t_0 \leq t < t_1$

When $t = t_0$, the hybrid energy storage module is fully charged to a voltage of 23.6 V. The brushless DC motor is still operating and its voltage is maintained at 47.5 V but the current fluctuates. Then, when $t_0 < t < t_1$, the photovoltaic module is disconnected to make $P_{pv} < P_{load}$, and its current gradually decreases, indicating that there is insufficient power to charge the hybrid energy storage module. At this time, owing to the disconnection of the photovoltaic module, the hybrid energy storage module continues to discharge to operate the motor. Thus, the brushless DC motor still runs and its voltage remains at 47.5 V (Fig. 10).

(3) $t_1 \leq t \leq t_2$

When $t = t_1$, the hybrid energy storage module discharges. The voltage of the hybrid energy storage module is 23.6 V and the current is 5.6 A. The brushless DC motor still operates and its voltage remains at 47.5 V. Then, when $t_1 < t < t_2$, the hybrid energy storage module still discharges and the brushless DC motor operates with its voltage remaining at 47.5 V. When $t = t_2$, the hybrid energy storage module discharges and its voltage drops to 19.6 V. Then, the hybrid energy storage module is disconnected to avoid the over-discharge of the lithium-ion battery module. At this time, the current of the hybrid energy storage module is 11.2 A (Fig. 11).

When $t_0 \leq t \leq t_2$, the hybrid energy storage module discharges, and the load of the system maintains the required voltage if $P_{pv} < P_{load}$. This indicates that the hybrid energy storage module supplies power continuously. The total discharge time is about 342 s.

4.2 Supercapacitor

We test the system only with a supercapacitor. The result is shown in Fig. 12. The measurement results of control strategies 1 and 2 are shown in Figs. 13 and 14, respectively.

First, control strategy 1 is implemented to establish whether the supercapacitor stores a similar quantity of power to that required by the brushless DC motor. As shown in Fig. 13, when

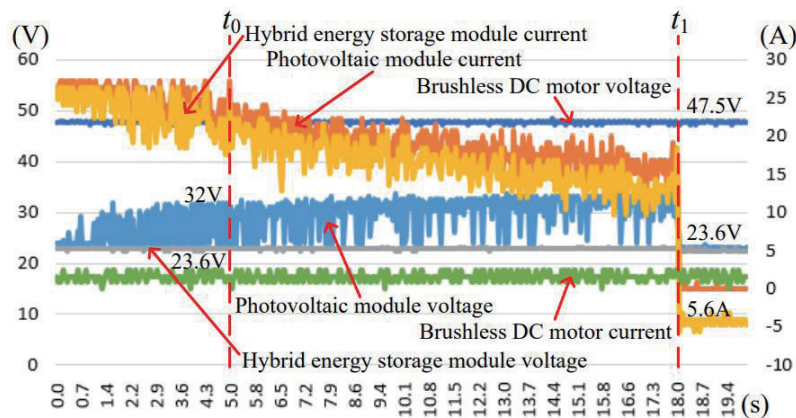


Fig. 10. (Color online) Control strategy 2: $t_0 \leq t < t_1$.

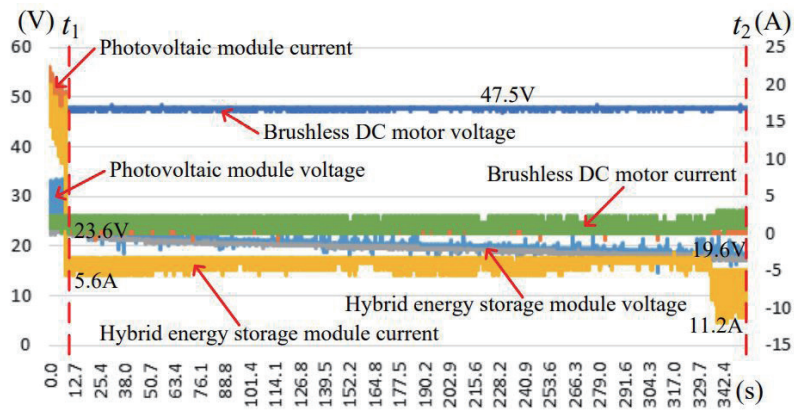


Fig. 11. (Color online) Control strategy 2: $t_1 \leq t < t_2$.

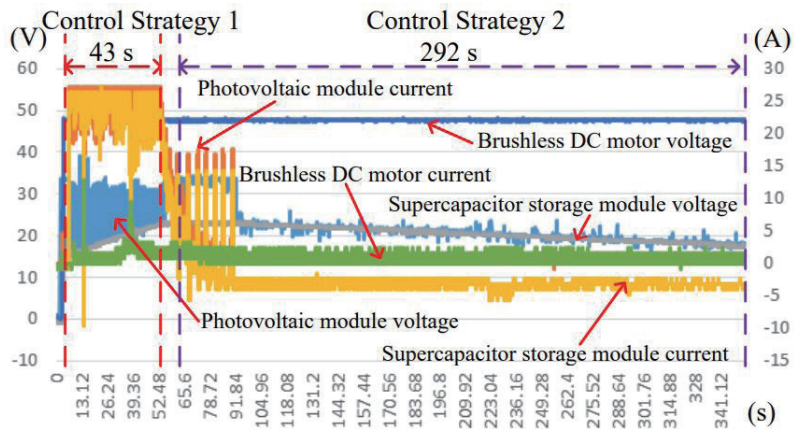


Fig. 12. (Color online) Solar energy storage system with only the supercapacitor storage module – complete measurement waveform.

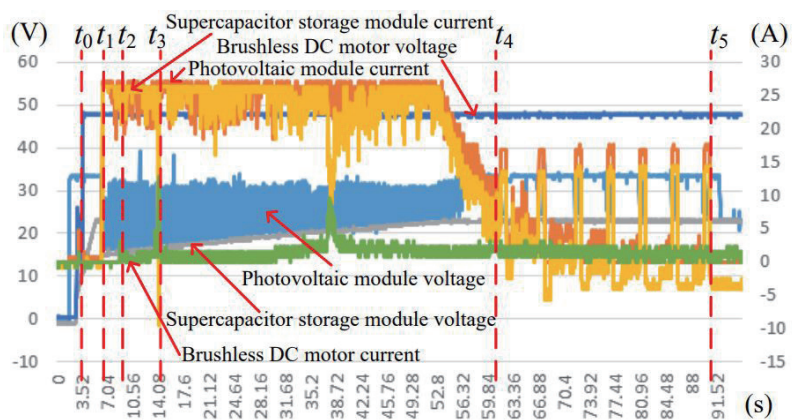


Fig. 13. (Color online) Solar energy storage system with only the supercapacitor storage module – control strategy 1.

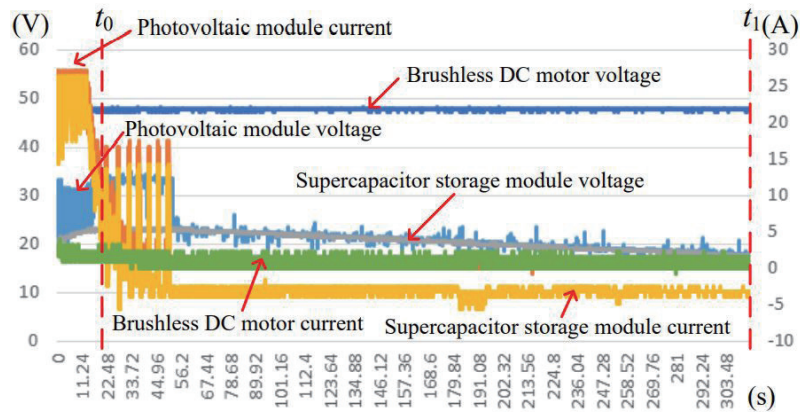


Fig. 14. (Color online) Solar energy storage system with only the supercapacitor storage module – control strategy 2.

Table 2

Measurement results of the hybrid energy storage module.

	Hybrid energy storage module	Supercapacitor
Initial charging voltage (V)	20	18
Charging cutoff voltage (V)	23.6	23.6
Charging time (s)	75	43
Discharging cutoff voltage (V)	19.6	20
Discharging time (s)	342	292

$t = t_3$ and $t_4 \leq t < t_5$, the power from the photovoltaic module and the supercapacitor is sufficient for the brushless DC motor to run. Thus, the photovoltaic power generation system charges the supercapacitor and operates the brushless DC motor when $P_{pv} > P_{load}$. When the initial voltage of the supercapacitor storage module is 18 V, the required charging time is about 43 s. When $P_{pv} < P_{load}$, the supercapacitor discharges and the brushless DC motor maintains the required voltage, indicating that the supercapacitor acts as an uninterruptible power supply with a total discharge time of about 292 s.

4.3 Comparison of results of hybrid energy storage module and supercapacitor

The required charging time and the time to maintain the brushless DC motor of the energy storage modules are compared in Table 2. The results are consistent with the control strategies. The results also show that the proposed hybrid energy system and the supercapacitor operate the brushless DC motors effectively. However, the total operation time of the hybrid energy storage module is longer than that of the supercapacitor.

5. Conclusions

The proposed hybrid energy storage module with lithium-ion batteries and a supercapacitor reduces the voltage instability and intermittency of the power output, provides a sustainable

power supply, and maintains the power quality of the photovoltaic power generation system. Therefore, the photovoltaic power generation system operates a brushless DC motor effectively. The experimental results show that the initial charging voltage of the hybrid energy storage module is 20 V and increases to 23.6 V with a charging time of 75 s. The brushless DC motor operates for up to 342 s with the hybrid energy storage module. The initial charging voltage of the supercapacitor alone is 18 V, which is charged to 23.6 V with a charging time of 43 s. Then, the brushless DC motor operates for about 292 s. The total operation time of the brushless DC motor in the hybrid energy storage module is longer than that of the supercapacitor. The results indicate that the hybrid energy storage module prolongs the operation time of the brushless DC motor and allows the photovoltaic power generation system to supply more stable power than other energy storage modules.

Acknowledgments

This research was partially supported by the Ministry of Science and Technology of Taiwan under Grant MOST 109-2622-E-167-016.

References

- 1 M. Z. S. El-Dein, M. Kazerani, and M. M. A. Salama: IEEE Trans. Sustainable Energy **4** (2013) 145. <https://doi.org/10.1109/TSSTE.2012.2208128>.
- 2 U. Manandhar, N. R. Tummuru, S. K. Kollimalla, A. Ukil, G. H. Beng, and K. Chaudhari: IEEE Trans. Ind. Electron. **65** (2018) 3286. <https://doi.org/10.1109/TIE.2017.2750622>.
- 3 N. Liu, Q. Chen, X. Lu, J. Liu, and J. Zhang: IEEE Trans. Ind. Electron. **62** (2015) 4878. <https://doi.org/10.1109/TIE.2015.2404316>.
- 4 W. Mao, X. Zhang, R. Cao, F. Wang, T. Zhao, and L. Xu: IEEE Trans. Ind. Electron. **65** (2018) 2653. <https://doi.org/10.1109/TIE.2017.2736483>.
- 5 M. B. Shadmand, R. S. Balog, and M. D. Johnson: IEEE Trans. Sustainable Energy **5** (2014) 1434. <https://doi.org/10.1109/TSSTE.2014.2345745>.
- 6 K. Yao, S. Chen, M. Rahimabady, M. S. Mirshekarloo, S. Yu, F. E. H. Tay, T. Sritharan, and L. Lu: IEEE Trans. Ultrason. Ferroelectr. Freq. Control **58** (2011) 1968. <https://doi.org/10.1109/TUFFC.2011.2039>.
- 7 S. Subramanian, M. A. Johny, M. M. Neelanchery, and S. Ansari: IEEE Trans. Power Electron. **33** (2018) 10410. <https://doi.org/10.1109/TPEL.2018.2810889>.
- 8 J. R. Miller: IEEE Electr. Insul. Mag. **26** (2010) 40. <https://doi.org/10.1109/MEI.2010.5511188>.
- 9 K. Liu, C. Zhu, R. Lu, and C. C. Chan: IEEE Trans. Plasma Sci. **41** (2013) 1267. <https://doi.org/10.1109/TPS.2013.2251363>.
- 10 A. Kuperman, M. Mellincovsky, C. Lerman, I. Aharon, N. Reichbach, G. Geula, and R. Nakash: IEEE Trans. Power Electron. **29** (2014) 5399. <https://doi.org/10.1109/TPEL.2013.2292674>.
- 11 R. German, A. Hammar, R. Lallemand, A. Sari, and P. Venet: IEEE Trans. Power Electron. **31** (2016) 548. <https://doi.org/10.1109/TPEL.2015.2408457>.
- 12 M. Uno and A. Kukita: IEEE Trans. Power Electron. **30** (2015) 3077. <https://doi.org/10.1109/TPEL.2014.2331312>.
- 13 R. P. Deshpande: Ultracapacitors (McGraw Hill, 2014, New Delhi).
- 14 A. Kuperman, M. Mellincovsky, C. Lerman, I. Aharon, N. Reichbach, G. Geula, and R. Nakash: IEEE Trans. Power Electron. **29** (2014) 5399. <https://doi.org/10.1109/TPEL.2013.2292674>.
- 15 A. Lahyani, P. Venet, A. Guermazi, and A. Troudi: IEEE Trans. Power Electron. **28** (2013) 1509. <https://doi.org/10.1109/TPEL.2012.2210736>.
- 16 R. German, A. Hammar, R. Lallemand, A. Sari, and P. Venet: IEEE Trans. Power Electron. **31** (2016) 548. <https://doi.org/10.1109/TPEL.2015.2408457>.
- 17 A. Soualhi, M. Makdessi, R. German, F. R. Echeverría, H. Razik, A. Sari, P. Venet, and G. Clerc: IEEE Trans. Ind. Inf. **14** (2018) 24. <https://doi.org/10.1109/TII.2017.2701823>.

- 18 Z. Li, C. Zhu, J. Jiang, K. Song, and G. Wei: *IEEE Trans. Power Electron.* **32** (2017) 3301. <https://doi.org/10.1109/TPEL.2016.2584701>.
- 19 M. X. Zheng, B. J. Qi, and H. J. Wu: 2008 3rd IEEE Conf. Industrial Electronics and Applications (IEEE, 2008) 1180–1184.
- 20 A. Jossen: *J. Power Sour.* **154** (2006) 530. <https://doi.org/10.1016/j.jpowsour.2005.10.041>.
- 21 A. A. A. Ismail and A. Elnady: *IEEE Access* **7** (2019) 54167. <https://doi.org/10.1109/ACCESS.2019.2912315>
- 22 W. Jiang, P. Wang, Y. Ni, J. Wang, L. Wang, and Y. Liao: *IEEE Trans. Ind. Electron.* **65** (2018) 2975. <https://doi.org/10.1109/TIE.2017.2752126>.
- 23 J. S. Park, K. D. Lee, S. G. Lee, and W. H. Kim: *IEEE Trans. Power Electron.* **34** (2019) 3020. <https://doi.org/10.1109/TPEL.2018.2868828>.
- 24 A. V. Stepanov and V. N. Enin: 2019 Int. Ural Conf. Electrical Power Engineering (UralCon, IEEE, 2019) 277–283.
- 25 G. Liu, X. Chen, X. Zhou, and S. Zheng: *IEEE Trans. Ind. Electron.* **67** (2020) 6158. <https://doi.org/10.1109/TIE.2019.2950857>.